RSC Advances

ROYAL SOCIETY OF CHEMISTRY

www.rsc.org/advances

Journal Name

ARTICLE

Photophysical and Charge Transport Properties of Pyrazolines

Joseph Ajantha,[ab] Elumalai Varathan,[abc] Vishal Bharti,[bcd] Venkatesan Subramanian,[*abc] Shanmugam Easwaramoorthi,[*abc] Suresh Chand[bcd]

Received 00th January 2015,
Accepted 00th January 2015

DOI: 10.1039/x0xx00000x

www.rsc.org/

Pyrazolines, an intense green emitting molecule both in solution and solid state with extended π–conjugation has been synthesized via simple, two step reactions in higher yields. Being with electron rich pyrazoline moiety with good redox behavior, pyrazolines can be a potential candidate for charge transport material in organic electronic devices. UV-visible absorption spectra of pyrazolines falls under 400 nm, a desired feature expected for charge transport material as it would avoid interference with donor absorption which falls on visible to NIR region. Further, electrochemical and theoretical studies shows that the HOMO energy level lies around -4.8 to -5.2 eV depending upon the substitutions, which is in fact compatible with the PEDOT:PSS/P3HT and work function of the ITO electrode. The experimental hole transport value measured using the hole only device and space charge limited current (SCLC) method was found to be in the range of 10^{-5} to 10^{-6} $cm^2V^{-1}s^{-1}$ depending upon the substitution.The maximum hole mobility calculated by theoretical methods for the pyraolines corresponds to 0.75 $cm^2V^{-1}s^{-1}$.

Introduction

Electron rich, π-conjugated organic molecules play crucial role in optoelectronic devices such as donor molecules in organic photovoltaics (OPV) and sensitizer in dye-sensitized solar cells (DSSCs), emitters in organic light-emitting diodes (OLEDs), charge transporting materials in OPV, DSSC, and OLEDs due to their flexibility in designing the molecules with the desired properties, established standard protocols, and relatively low cost large scale synthesis, etc. Nonetheless, the critical aspect limiting a faster progress in organic photovoltaics is due to the inherent difficulty in generation and transport of charge carrier.[1, 2] The stacked structure of organic photovoltaic devices not only involve the charge transport within the material, but even more competition in the charge transfer is experienced at the interface between different materials, namely electrode/organic[3], inorganic/organic[4] or organic/organic heterojunctions.[5] In order to overcome this problem, charge carriers for transporting either hole or electron or both (ambipolar) across the interfaces become crucial. They decide the overall efficiency of the devices due to many reasons such as smoothing of the electrode surface, protecting the active layer from the electrode, and blocking excitons.[6] An impressive progress has been made by several research groups in developing the charge carriers with high carrier mobility, stability, and durability. Most efficient and commonly used polymer based hole transport material is poly (3,4-ethylenedioxythiophene) : poly(styrenesulfonate) (PEDOT:PSS) due to its smooth anode surface, reduced current leakage, and higher device stability. However hygroscopicity,[7] unstable morphology,[8] electrical inhomogeneity,[9] intrinsic acidity, weak electron blocking,[10] low LUMO level[11] of PEDOT:PSS restricts its application as an ideal hole transport material. Several attempts have been made to find alternative hole transport materials to PEDOT:PSS, which include metal oxides such as molybdenum oxide (MoO_3),[12] nickel oxide (NiO_x),[13] vanadium oxide (V_2O_5).[14] The metal oxides have the capability to align with a wide range of energy levels, enabling them to form low-resistance ohmic contacts with the organic materials, high transparency, desirable band structure and excellent stability in ambient conditions, which can extend the lifetime of organic electronics.[15] However, harsh experimental conditions such as high-temperature annealing[16] and vacuum deposition process required for metal oxides makes them incompatible with the solution processes, and thus limits their practical applications. Thus, it is desirable to develop suitable alternatives having better air and thermal-stability, compatible with solution-processable fabrication of solar cells. In this regard, a variety of small molecules has been developed as charge carriers, such as triarylamine derivatives,[17,18] spirothioxanthene,[19] phenothiazine[20] and spiro-OMeTAD.[21,22,23] Among them, triphenylamine (TPA) derivatives have been widely used as HTMs because of their efficient hole mobilities, high electron donating property, excellent stability.[24,25] The charge carrier mobility of spiro-OMeTAD was found to be 10^{-5} cm^2 V^{-1} S^{-1} to close to 10^{-3} cm^2 V^{-1} S^{-1} values.[26,27] One of the limitations that has been suggested is the low hole mobility of spiro-OMeTAD causing excessive interfacial recombination losses.[28,29] Spiro-OMeTAD continues to be the best performing candidate for HTM, but its higher cost associated with

[a] Chemical Laboratory, CSIR-Central Leather Research Institute, Adyar, Chennai – 600020, India. E-mail: moorthi@clri.res.in. Fax: +91-44-24411630.
[b]. CSIR-Network of Institutes for Solar Energy (NISE), CSIR-NPL, New Delhi, India.
[c] Academy of Scientific and Innovative Research (AcSIR).
[d] Physics of Energy Harvesting Division, National Physical Laboratory, K. S. Krishnan Marg, New-Delhi - 110012, India.

† Electronic Supplementary Information (ESI) available: Characterization, UV-visible, fluorescence spectral details. DOI: 10.1039/x0xx00000x.

difficulties in its synthesis slow down the growth and advancement of high efficiency solar cells.

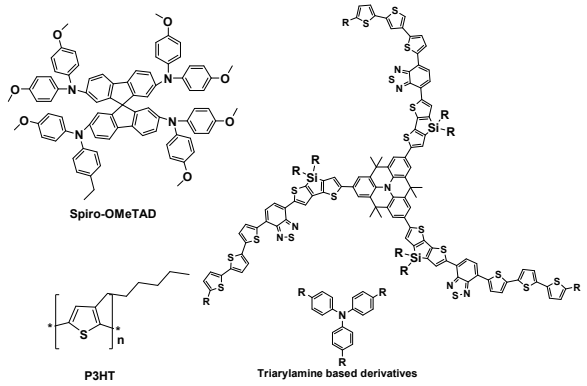

Chart 1 Molecular structures of different HTMs.

In this report, we have studied the photophysical and hole transport properties of a new class of compounds based on pyrazoline skeleton. We have synthesized four pyrazolines with methoxy and allyloxy substituents at different positions. Pyrazolines, a well-known brightening agent,[27] are widely used in biological systems, synthetic fibers, fluorescent probes, chemosensors, hole transport material,[30,31] electro photography, and electroluminescence[32,33] owing to their stronger fluorescence and blue emitting property. Pyrazoline derivatives are synthetically accessible, thermally and environmentally stable and absorb at considerably shorter wavelength. The pyrazoline derivatives with high glass transition temperature (T_g) have been known as excellent hole transport material in organic electroluminescent device.[34,35] Higher hole mobilities in pyrazoline doped polymers have also been reported.[36] Polymer based hole transport materials have advantages like chemical and thermal stability, these molecules have disadvantage of poor solubility and lower power conversion efficiency. Different electron donating groups have been selected to unravel hole transport property in organic solar cells. Their unique properties such as rich electron density, ease of modulation of redox behavior, excellent spectral properties along with the judicious choice of substituents have been the criteria for efficient hole transporting materials. In particular, their influences on their electronic energy levels and ionization potentials have been investigated to develop better hole-transport materials. Both experimental and theoretical approaches have been employed in order to characterize the synthesized compounds and to understand the structure-property relationships.

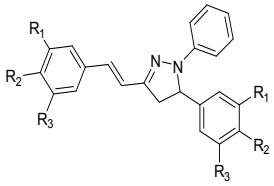

	R_1	R_2	R_3
1a	H	OCH_3	H
1b	H	OCH_2CHCH_2	H
1c	H	OCH_3	OCH_3
1d	OCH_3	OCH_3	OCH_3

Chart 2

Results and Discussion

Synthesis of the pyrazolines was accomplished by a simple, efficient, two-step process outlined in Scheme 1. The intermediate compound 1,5-diphenylpenta-1,4-dien-3-one derivatives (B) and pyrazolines were synthesized according to the reported procedure.[37, 38] Briefly, Claisen-Schmidt condensation of 1 mole of acetone with 2 moles of substituted aromatic aldehyde (C) in 30 mL of ethanol affords the corresponding 1,4-dien-3-one derivative 'B' in excellent yields (90-95 %). Further treatment of 'B' with excess phenyl hydrazine in acetic acid produces pyrazolines (A) as yellow solid in 80-85 % yield and the crude product was purified by column chromatography over silica gel using hexane and ethylacetate (90:10, v/v) as eluent.

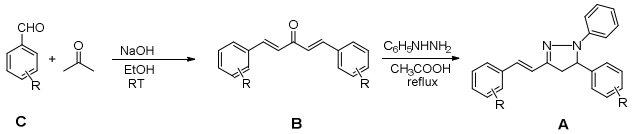

Scheme 1 Synthesis of 1,5-diphenyl-3-styryl-4,5-dihydro-1H-pyrazole derivatives.

The IR spectra of dibenzylideneacetones exhibits characteristic absorption bands corresponding to α, β -unsaturated ketone (1650 - 1680 cm^{-1}) and trans C=C (970 - 990 cm^{-1}). Pyrazolines shows characteristic absorption bands in FTIR spectrum at 1590 - 1600 cm^{-1} and 1310-1330 cm^{-1}, due to C=N and C–N moieties, respectively. The compounds were also characterized using ^1H and ^{13}C NMR spectra (SI).

Table 1 Thermal characteristics of compounds **1a-1d.**

Compound	^aT_g (˚C)	^aT_m (˚C)	T_{ID} (˚C)
1a	79	151	267
1b	NA	88	271
1c	95	142	286
1d	80	183	309

[a]Determined by DSC, scan rate 10°C/min, N_2 atmosphere. T_m, temperature at melting; Tg, glass-transition temperature; T_{ID}, thermal decomposition onset.

The thermal stability of the pyrazolines **1a-1d** is determined by DSC and TGA measurements (Fig. 1) and the data are given in Table 1. The glass transition temperatures of all the compounds are found to be in the range ~78 to 95°C except **1a**. A second heating scan was performed to detect the decomposition temperature (Td) by TGA. Decomposition temperature of pyrazolines measured from TGA is found to be above 290°C, which would enable these materials to be processed at elevated temperature during device fabrications. An endothermic peak observed at 88°C for **1b** in DSC has been

ascribed to the melting point of the system and the broad exothermic peak at 263°C indicates the thermal polymerization of allyloxy group.

Systematic UV-visible and fluorescence spectral studies are carried out to understand the electronic properties of pyrazolines. The UV-visible absorption spectra of **1a-1d** in acetonitrile shown in Fig. 2, results summarized in Table 2 indicate that there are no significant changes in the absorption spectrum except the molar extinction coefficient for different substituents. The lowest energy peak observed at 381 nm has been assigned to the transition from singlet ground (S_0) to the first singlet excited state (S_1) and the band at 275 nm is ascribed to $S_0 \rightarrow S_2$ transition.

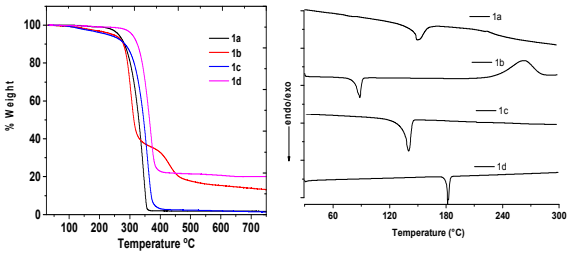

Fig. 1 TGA and DSC thermogram of pyrazolines 1a-1d scan rate of 10°C/min, N_2 atmosphere.

The absorption maximum of **1a**-**1d** is found to be red-shifted when compared to the structurally similar chromophores based on pyrazolinopiperidines, wherein the five membered pyrazoline ring is fused with the piperidine moiety.[38] This difference can be attributed to the enhanced planarity of the pyrazolines studied here than the reported compound which eventually increases the π-conjugation throughout the molecule and reduces the energy gap between the ground and first excited singlet state. Nevertheless, the absorption onset for the derivatives lies below 400 nm; hence it is not expected to interfere with the absorption of the donor materials of organic solar cells, which generally appears in the visible-NIR region. Further, **1a**-**1d** poses intense yellowish green fluorescence with a maximum at 475±5 nm both in solution and solid state.

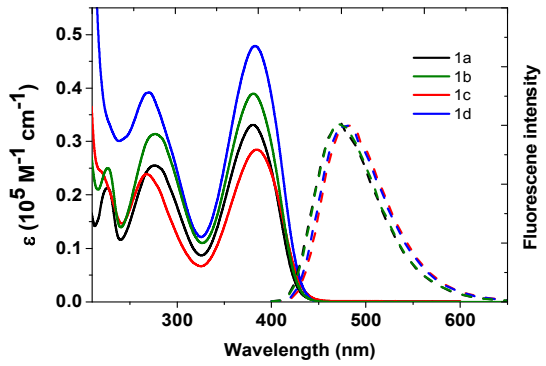

Fig. 2 UV-visible absorption and fluorescence emission of pyrazolines derivatives **1a-1d** in acetonitrile solvent.

Interestingly, **1a**-**1d** poses negligible overlap in absorption and fluorescence spectra as can be seen from Fig. 2 with larger Stokes shift values over 5000 cm^{-1}.

Non-overlapping absorption and emission spectra are highly desirable for a molecule to be used as fluorescent probes in microscopic applications. The fluorescence quantum yield is determined to be 0.19±0.2 with respect to quinine sulphate (0.05 M H_2SO_4) in water.[39] The fluorescence lifetimes were measured by exciting the sample at 375 nm with 100 ps pulsed light and the decay profiles monitored at respective emission maximum wavelength are given in Fig. S2. The decay profiles were fitted satisfactorily with single exponential function (ψ^2 = 1 to 1.2) and fluorescence lifetimes correspond to 2.95, 3.65, 2.84, 2.83 ns respectively for **1a**, **1b**, **1c**, and **1d**. The radiative and non-radiative rate constants calculated from fluorescence quantum yield and lifetime are found to be insensitive to the nature of the substituents (Table 2).

Table 2 Photophysical properties of pyrazoline derivatives in acetonitrile solvent.

Cmpd.	λ_{abs} nm (ε 10^4 $M^{-1}cm^{-1}$)	λ_{fl} nm	Stokes Shift (cm^{-1})	τ_{fl} (ns)	Φ_{fl}	K_r [10^8 s^{-1}]	K_{nr} [10^8 s^{-1}]
1 a	225 (2.14), 275 (2.13), 381 (3.30)	472	5060	2.95	0.19	0.56	2.77
1b	227 (2.49), 285 (3.14), 381 (3.91)	474	5150	3.65	0.18	0.49	2.24
1c	265 (2.38), 385 (2.86)	480	5270	2.84	0.17	0.53	2.63
1d	304 (3.90), 383 (4.80)	481	5320	2.83	0.19	0.61	2.62

Further, possibility of the intramolecular charge transfer interactions of these compounds are studied by measuring the steady state fluorescence spectra in solvents of different polarity. While the absorption spectra of pyrazolines **1a**-**1d** were found to be insensitive, the fluorescence spectra shows solvent polarity induced, red-shifted emission spectrum characteristic of intramolecular charge transfer interactions (SI, Fig. S1 & Table S1). In this case, the pyrazoline and styrene moieties are respectively expected to acts as a electron donor and acceptor components. This is also supported by the molecular orbital pictures of highest occupied (HOMO) and lowest unoccupied (LUMO) molecular orbitals, wherein electron density redistribution occurs during the HOMO→LUMO transition (*vide infra*). The data summarized in Table S1 indicates that number of methyl group do not have any significant effect on the intramolecular charge transfer interactions. The density functional theory (DFT) based calculations are carried out to gain insight into the structure property relationship of these pyrazoline materials. The calculated frontier molecular orbital (FMO) distributions of molecules are shown in Fig. 3.

Compound	HOMO	LUMO
1a	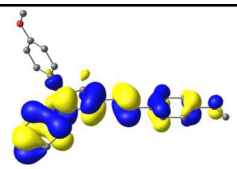	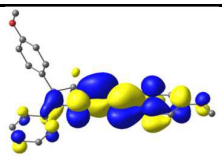
1b	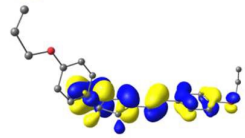	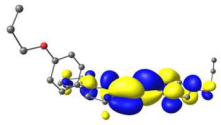
1c	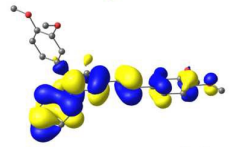	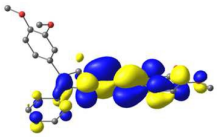
1d	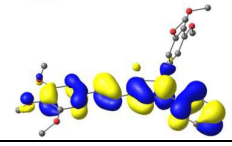	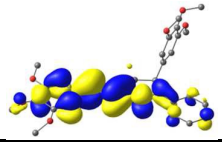

Fig. 3 Contour plots (isosurface value = 0.025 au) of the HOMO and LUMO levels of designed hole transport molecules at the B3LYP/6-31G* level. The hydrogen atoms are omitted here for clarity.

From the Fig. 3, it can be observed that both HOMO and LUMO are localized on the whole molecules. However, close analysis of these orbitals reveals that HOMO is predominantly localized on the pyrazoline moiety and LUMO is localized on the styrene unit. As a result, there is a possibility for the intramolecular charge transfer transition between the pyrazoline to styrene unit, which can also be understood from solvent polarity dependent fluorescence studies.

To understand the suitability of these molecules as charge carriers, electrochemical properties are studied using cyclic voltammetry and differential pulse voltammogram (DPV) using glassy carbon as working electrode, platinum wire as counter electrode and tetrabutylammonium hexafluorophosphate as supporting electrolyte. The energy of HOMO was calibrated using half wave potentials of ferrocene/ferrocenium redox couple which is -4.5 eV below vacuum.[40] The DPV of pyrazolines in homogeneous solution and films are given in Fig. 4 and the findings are summarized in Table 3. The first oxidation potentials of **1a**, **1b**, **1c**, and **1d** in acetonitrile solution are measured respectively to be 0.74, 0.62, 0.44, and 0.67 V with reference to Fc/Fc^+ redox couple. The first oxidation peak might have originated from the loss of electrons from pyrazoline nitrogen's. The HOMO values calculated from the electrochemical data based on the empirical formula HOMO = $-(E_{ox.\ onset}+ 4.5)$ (eV) corresponds to –5.24, –4.88, –5.02, –5.07 eV respectively for **1a**, **1b**, **1c**, and **1d**.

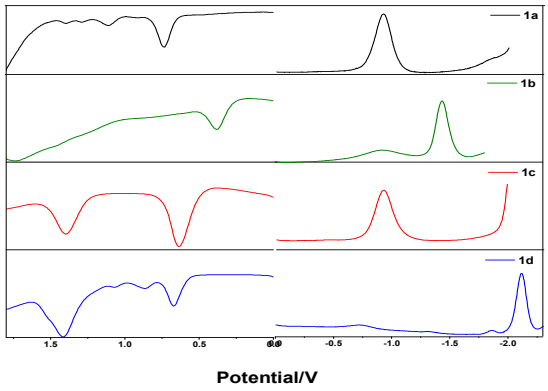

Fig. 4 Differential pulse voltammograms (dpv) of pyrazolines **1a-1d** (10 −3 M solutions, scan rate of 100 mV s −1 vs Ag/Ag+) in 0.1 M solution of tetrabutylammonium hexafluorophosphate in acetonitrile.

Table 3 Electrochemical, theoretical HOMO–LUMO and free energy changes for electron transfer process of pyrazolines.

Comd.	$^aE_{ox}$(V)	$^aE_{red}$ (V)	$^bE_{HOMO}$ (eV)	$^bE_{LUMO}$ (eV)	^cE_g (eV)	$^dE_{HOMO}$ (eV)	$^dE_{LUMO}$ (eV)	^eE_g(eV)	^fE_g (eV)
1a	0.74	-0.92	-5.24	-3.58	-1.6	-4.59	-1.38	-3.21	-2.75
1b	0.38	-1.43	-4.88	-3.07	-1.8	-4.57	-1.37	-3.20	-2.74
1c	0.62	-0.93	-5.02	-3.47	-1.5	-4.54	-1.33	-3.21	-2.71
1d	0.67	-2.12	-5.07	-2.28	-2.7	-5.47	-2.23	-3.24	-2.77

[a]The redox potential of compounds obtained from differential pulse voltammogram using glassy carbon as working electrode with reference to Fc/Fc^+ couple. 0.1 M Tetrabutylmmonium hexaflurophosphate was used as a supporting electrolyte. [b]$E_{HOMO/LUMO}$ HOMO and LUMO energy levels calculated from the redox potentials. [c]Eg = electrochemical HOMO–LUMO energy gap. [d]HOMO, LUMO energy calculated using Gaussian 09 programme at B3LYP/6-31G level. [e]Computed HOMO–LUMO energy gap. [f]Optical HOMO–LUMO energy gap (Zero–Zero transition energy estimated from the point of intersection of normalized absorption and emission spectra in acetonitrile).

These values are in accordance with the work function of the ITO electrode (4.5-4.7 eV) and also comparable to the HOMO of widely used hole transport material PEDOT: PSS (5.1-5.4eV).[41] Further, significantly higher HOMO energy level of **1a**-**1d** than the acceptor PCBM (HOMO = –6.10 eV; LUMO = –3.70 eV),[42] is expected to facilitate the electron transfer process between the hole transport layer and acceptor layer. The electrochemical stability of the components was understood from the constant redox behavior upon repeated reduction-oxidation cycles. HOMO-LUMO band gaps for **1a**, **1b**, **1c**, and **1d** calculated from electrochemical methods are found to be 1.66, 1.81, 1.50, and 2.79 eV respectively, which are in closer agreements with those obtained by optical method. Energy level diagram of the components are shown in Fig 5.

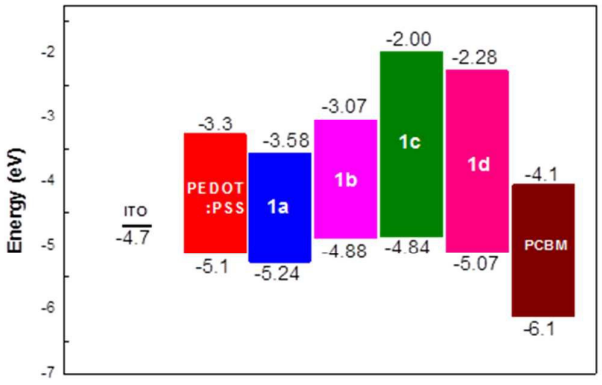

Fig. 5 Energy level diagram of the corresponding materials in BHJ OSCs.

The charge-carrier (hole and electron) mobility is a key factor in deciding the efficiency of organic solar cells. It has been evident from the previous studies that the charge mobility of organic molecules can be well described by the incoherent hopping model,[1, 43-45] where charge transport is viewed as a charge exchange reaction:

$$M^{n} + M^{i} \rightarrow M^{i} + M^{n} \quad \ldots\ldots\ldots\ldots [1]$$

Where, M^{n} represents the neutral state of the system and M^{i} represents the ionic state of the system. The hole/electron transfer rate can be expressed by the standard Marcus-Hush equation (2).[46-48]

$$K_{\text{hole/electron}} = \left(\frac{4\pi^2}{h}\right) \frac{1}{\sqrt{4\pi k_B T\, \lambda_{\text{hole/electron}}}} V^2 \exp\left(-\frac{\lambda_{\text{hole/electron}}}{4k_B T}\right) \ldots\ldots\ldots [2]$$

Where *T* is the temperature, *λ* is the reorganization energy, *V* is the electronic coupling matrix element (transfer integral) between neighboring molecules in the organic single crystal, *h* is the Planck constant and k_B is the Boltzmann constant. It is evident from the equation 2 that there are two key parameters which determine the charge transfer rate, λ and *V*. Theoretical investigations on the charge transport properties of several organic materials imply that both V and λ are equally responsible for the charge transfer properties. Hence, these two parameters need to be properly tuned to obtain the desired properties. Molecules having maximum transfer integral with minimum V_{ab} are expected to show optimal transport properties. The total reorganization energy of the molecule is given by the sum of internal and external reorganization energies. The former term involves the contributions from intramolecular geometry vibrations and the latter term describes the change in electronic polarization of the surrounding medium. The external reorganization energy can be neglected because most of the organic materials have low polarity and therefore the main contribution to the total reorganization energy would be from internal reorganization. In this study the internal reorganization energy (for hole and electron) is calculated by using the equations (3) and (4) and is schematically depicted in Scheme 2.

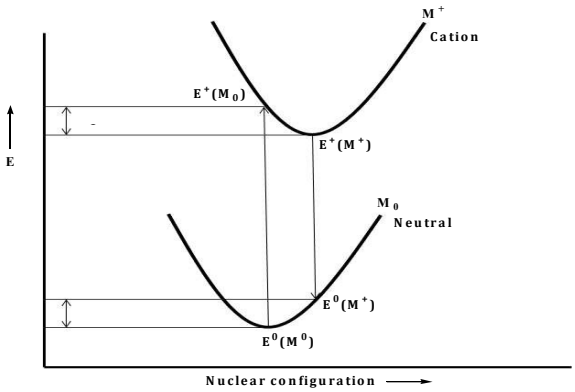

Scheme 2 Internal Reorganization Energy for Hole (λ_h) in Arbitrary Units

$$\lambda_+ = \lambda_1 + \lambda_2 \ldots\ldots\ldots [3]$$
$$\lambda_- = \lambda_3 + \lambda_4 \ldots\ldots\ldots [4]$$

$$\lambda_1 = E^+(M_0) - E^+(M^+); \quad \lambda_1 = E^0(M^+) - E^0(M_0)\ \lambda_3 = E^-(M_0) - E^-(M^+); \quad \lambda_1 = E^0(M^+) - E^0(M_0)$$

Where $E^0(M_0)$, $E^+(M^+)$, and $E^-(M^-)$ respectively denote the total energy of neutral, cationic, and anionic species at their optimized geometries. $E^+(M_0)$ and $E^0(M^+)$ denote the total energy of the cationic and neutral species at their optimized geometry of M_0 and M^+ respectively. Similarly, $E^-(M_0)$ and $E^0(M^-)$ represent the total energy of the anionic and neutral species at the optimized geometry of M_0 and M^- respectively. The reorganization energies for electrons (λ_-) and holes (λ_+) of the molecules were computed at the B3LYP/6-31G* level using Gaussian 09 program.[49, 50] It has been evident from the previous studies that B3LYP functional with 6-31G* basis set provides most reliable results on the reorganization of organic molecules.[25, 48, 51-53]

The transfer integral V_{ab} represents the strength of electronic coupling between the two adjacent neighboring molecules a and b. V_{ab} can be calculated based on Koopmans' theorem[54] by assuming that the interacting molecules are identical, symmetrically equivalent and also have the same site energies. This method have been most frequently used in the literature for the estimation of transfer integrals in organic semiconductors.[1]

$$V_{ab} = \frac{E_{H/L+1} - E_{H-1/L}}{2} \quad \ldots\ldots\ldots [5]$$

Where $E_{H/L+1}$ and $E_{H-1/L}$ are the energies of HOMO/LUMO+1 and HOMO-1/LUMO, respectively, obtained from the closed shell configuration of neutral state of two stacked pyrazolines molecules. Once the charge transfer rate is obtained by eqn. (2), the hopping mobility can be estimated by the Einstein relation, equation (6).

$$\mu_{\text{hop}} = \frac{eD}{k_B T} \quad \ldots\ldots\ldots\ldots [6]$$

Where T is temperature, k_B is Boltzmann constant, and D is the diffusion coefficient. The relation between D and k_{ct} for a one dimensional system is given by D = $l^2 k_{ct}$, where *l* is the space distance between two interacting molecules.

Reorganization energy (λ) is one of the important factors that govern the charge mobilities of the organic semiconductors. According to Marcus-Hush theory, lower λ value is expected to yield higher charge mobility. Hence, understanding the geometric deformation becomes vital as it has significant influence on the reorganization energy of organic molecules. The calculated reorganization energies of pyrazoline molecules are listed in Table 4. The electron reorganization energy (λ_-) is calculated to be 0.49, 0.54, 0.50, and 0.54 eV respectively for **1a**, **1b**, **1c**, and **1d**. Similarly the hole reorganization energy (λ_+) is found to be 0.32, 0.33, 0.35, and 0.43 eV respectively for **1a**, **1b**, **1c**, and **1d**. For all the molecules studied here, the magnitude of the electron reorganization energy (λ_-) is found to be profoundly larger than its corresponding hole reorganization energy (λ_+). This observation points out that the pyrazolines could be a good hole transport materials rather than the electron transport materials. We have also examined effect of substituent on λ_+ values. It can be seen that **1a** and **1b** have comparatively lower hole reorganization energy than the **1c** and **1d.** The slightly higher reorganization energy for **1d** than **1a** is due to the slight deviation from planar geometry by adding more substituents on R_1, R_2 and R_3 positions.

Table 4 Calculated Hole (λ_+) and Electron (λ_-) Reorganization Energies of hole transporting materials at B3LYP/6-31G* Level (Energies in eV).

Compound	Hole			Electron		
	λ_1	λ_2	λ_+	λ_3	λ_4	λ_-
1a	0.16	0.15	0.32	0.25	0.24	0.49
1b	0.17	0.16	0.33	0.25	0.28	0.54
1c	0.19	0.16	0.35	0.25	0.25	0.50
1d	0.23	0.20	0.43	0.26	0.28	0.54

The charge transfer integral (V_{ab}), a parameter that defines the electronic coupling between the two molecules has been influenced by the way of intermolecular stacking. Though the molecular stacking can generate a large number of conformations, being with extended π–conjugation, the intermolecular stacking is expected to be dominantly influenced by the π–π interactions.

Indeed, face to face π-stacking with a large orbital overlap facilitates the enhanced electronic coupling between the two adjacent molecules and consequently aids the inter-chain charge transport of an organic molecule. In absence of any experimental results, two different methodologies have been used to compute the transfer integral (V_{ab}). In one of the method, the initial geometry of the two monomers is co-facially stacked at the distance of ~3.5 Å, and then the structures are further optimized. The orbital energies required for charge transfer integral calculation are obtained from the optimized geometries. In the second case, the single point calculations of the two monomers are co-facially stacked at the distance of ~3.5 Å. Electronic coupling values of all the dimers are calculated for the optimized structures of two adjacent dimers obtained at the M05-2X/6-31G* level of theory. Optimized structures of the dimers are shown in Fig. 6.

Charge transfer integrals (V_{ab}), charge transfer rates (K), and hopping mobilities (μ) are calculated respectively using equations 5, 2, and 6, for all the dimers and results are given in Table 5. The above calculations are performed at room temperature (298 K). As shown in the Table 5, both the charge transfer rate and the mobility have the same trend. Both are larger for hole compared to electron, except for system **1c**. Hence, these molecules might be the good hole transport materials. The quite larger K and μ values for hole compared to electron is due to small hole reorganization energies and larger electronic coupling. The calculated carrier mobility is quite consistent with the experimental values (*vide infra*). However, theoretical values provide an upper limit of the charge mobility values compared with experimentally reported one although, the trends remains same.

Table 5 The charge transfer integrals (V_{ab} in eV) and the average intermolecular distance (in Å) for the M05-2X/6-31G* geometries optimized of the lowest energy dimer, reorganization Energy (λ), Maximum Transfer Integral (t), Maximum Rate of Charge Hopping (K), and Drift Mobility (μ) for Hole and Electron of hole transporting materials.

				V_{ab} (eV)		K (s^{-1})		μ ($cm^2 V^{-1} s^{-1}$)	
	λ_+ (eV)	λ_- (eV)	D (Å)	h^+	e^-	h^+ x10^{12}	e^- x10^{11}	h^+	e^-
1a	0.32	0.49	3.39	0.096	0.09	12.1	16.5	0.54	0.07
1b	0.33	0.54	2.73	0.148	0.14	25.8	23.3	0.75	0.06
1c	0.35	0.50	3.98	0.006	0.03	0.03	0.16	0.002	0.01
1d	0.43	0.54	4.33	0.107	0.06	4.46	0.43	0.33	0.03

To understand the influence of charge carrier transport on photovoltaic performance, we used space charge limited current (SCLC) method to measure the hole mobility in the blend. Fig. 7 shows the *J-V* curves for hole only device configuration. The hole transport properties of pyrazolines **1b**-**1d** are evaluated by measuring the charge carrier mobilities using hole only device configuration viz. indium tin oxide (ITO)/poly(3,4-ethylendioxythiophene)-poly(styrene sulfonate) (PEDOT:PSS)/Hole transport layer (**1b**, **1c** and **1d**)/Au. PEDOT: PSS was spin-coated onto the cleaned ITO substrate and dried at 140°C for 30 min in a vacuum.

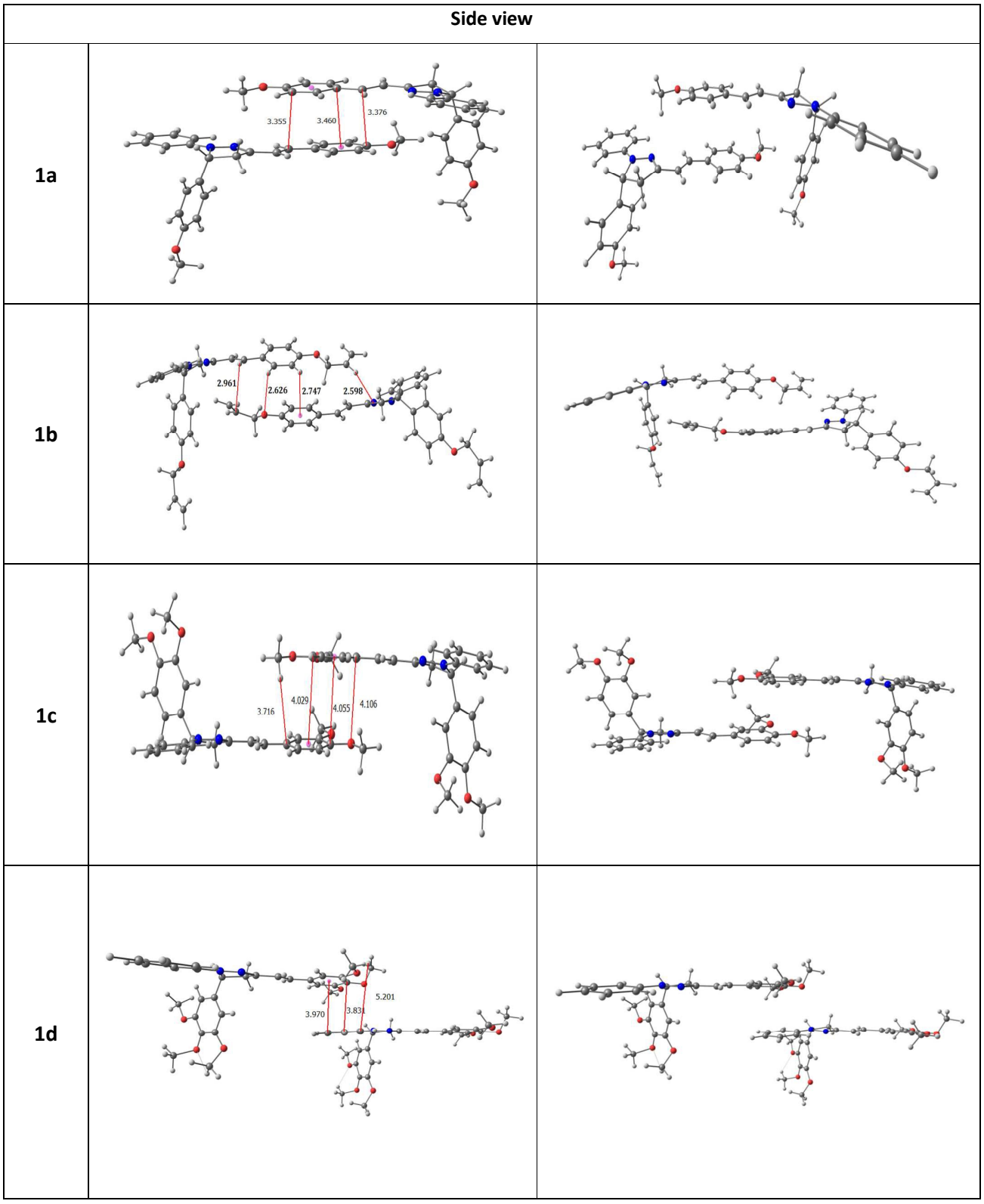

Fig. 6 Optimized geometry of dimers using M05-2X/6-31 method

The role of PEDOT:PSS layer (40 nm) reduces the roughness of ITO as well as improves the work function to achieve a better hole only device properties. These active materials **1b**, **1c** and **1d** spin coated onto PEDOT:PSS from chloroform solution (40 mg/ml) in the glove box. Finally, Au contacts (200 nm thick) were applied via thermal evaporation through a shadow mask in 8×10^{-6} Torr vacuum. The work function of Au and ITO are close to the HOMO energy level of HTL materials as well as far below the LUMO energy level. Therefore the electron injection barrier is quite high when compared to the hole injection barrier, from both the electrodes. As a result, the transport is dominated by holes in the so-called hole only device. The J-V characteristics of these samples were measured with a Keithley 2420 Source Meter unit interfaced with a PC at room temperature.[55-57]

At low applied bias the J-V characteristics follow the Ohm's law [Fig. 7] as the injected holes density p is negligible when compared to the density of thermally generated holes inside the specimen. This is illustrated by the following equation:

$$qp_0\mu\frac{V}{d} > \frac{9}{8}\varepsilon\mu\frac{V^2}{d^3} \quad \text{.....[7]}$$

Where, q is the electronic charge, μ is the carrier mobility, d is the thickness of the film, and ε is the permittivity of material.

With the increase in applied voltage, the injected carrier density increases and a point is reached where it is equal to the thermally generated carrier density and the J-V characteristics hence follow the space charge limited conduction (SCLC) mechanism. The onset voltage (V_Ω) which governs the transition from Ohm's law to SCLC is given by

$$V_\Omega = \frac{8}{9}\frac{qp_0d^2}{\varepsilon} \quad \text{.....[8]}$$

when slope of the J-V characteristics is ~ 2 and then it follow the Mott-Gurney's equation is obeyed viz

$$J = \frac{9}{8}\varepsilon\mu\frac{V^2}{d^3} \quad \text{.....[9]}$$

The equation does not imply the absence of traps but reveals that up to a particular temperature thermal energy is sufficient to fill all the traps.

When the slope of the characteristics is > 2 and Eqn. (9) is not followed implying that now thermal energy is not sufficient to fill the traps. The J-V characteristics follow the trap limited conduction with traps distributed exponentially in energy and space and is given by:

$$J = q^{1-l}\mu N_v\left(\frac{2l+1}{l+1}\right)^{l+1}\left(\frac{l}{l+1}\frac{\varepsilon\varepsilon_0}{H_b}\right)^{l}\frac{V^{l+1}}{d^{2l+1}} \quad \text{.....[10]}$$

Where q is the elementary charge, μ is the charge carrier mobility, N_v is the effective density of states, d is the film thickness, ε is the dielectric constant of material, ε_0 is the permittivity of the free space; H_b is the total trap density at the edge of valence band.

The J-V characteristics of three samples viz. **1b**, **1c**, and **1d** are shown in Fig. 7. The experimental curve of **1b** and **1c** shows two regions of conduction that is Ohmic conduction at low voltage and trap limited conduction (non Ohmic conduction) at high voltage and **1d** shows trap free SCLC conduction at high voltage.

Table 6 Charge transport parameters in the samples generated by theoretical fitting of experimental curves.

Compd.	μ ($cm^2 V^{-1} s^{-1}$)	N_V (cm^{-3})	H_b (cm^{-3})	d (nm)
1b	1.5×10^{-6}	-	-	400
1c	3×10^{-6}	1×10^{18}	6×10^{17}	390
1d	4×10^{-5}	3×10^{18}	1.7×10^{17}	580

The theoretical curve generated using equation 10 have been found to be fit the experimental curve as shown in Fig. 7 with charge transport parameters as given below for all three samples. The hole mobility is measured to be 3×10^{-6}, 4×10^{-5}, and 1.5×10^{-6} $cm^2V^{-1}s^{-1}$ 1d is found to show higher hole mobility compare to 1b and 1c.

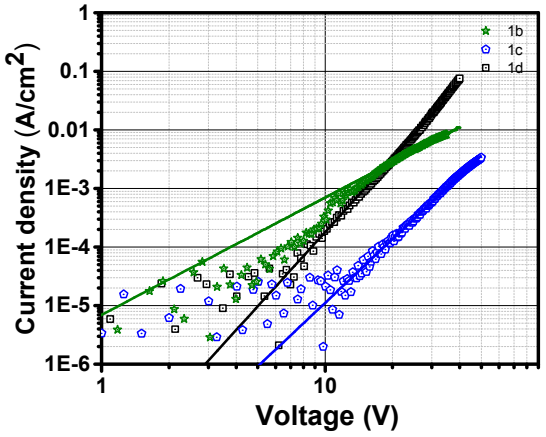

Fig. 7 *J-V* characteristics of devices experimental (symbols) and theoretical fit (solid lines using Eq. 3, 4).

Conclusion

Photophysical and hole transport properties of pyrazoline derivatives are studied by experimental and theoretical methods. Pyrazolines can be synthesized in good yields by simple, two step reactions using relatively cheap starting materials. The UV-visible absorption and fluorescence studies shows the intense green emission in both solid state and solution state having non-overlapping absorption and emission spectra, an important prerequisite for many fluorescence based applications. While the electronic properties are not significantly influenced by the substituents, their influence on the charge carrier mobilities can be correlated to their film forming abilities, reorganization energies. Further, optical, electrochemical, and theoretical measurements

shows that the HOMO energy levels of pyrazoline lies between –4.8 to –5.2 eV, which is ideal value to be used as a hole transport material. The highest charge carrier mobility measured using space charge limited current method is found to be in the order of $4X10^{-5}$ $cm^2V^{-1}s^{-1}$ for dimethoxy substituted phenyl moiety. The smaller reorganization energy for the hole than the electron suggests that pyrazolines can be a better hole transport materials. This result may provide a new way to further optimize the hole transport materials based on pyrazoline skeleton. Furthermore, the pyrazolines as HTM in this work is cost-effective, which can also avoid the complicated synthesis of triarylamine derivatives and significantly reduce the cost of devices.

AUTHOR INFORMATION

Corresponding Author

*moorthi@clri.res.in, subbu@clri.res.in

Author Contributions

The manuscript was written through contributions of all authors. All authors have given approval to the final version of the manuscript.

ACKNOWLEDGMENT

We acknowledge CSIR-TAPSUN (NWP-54) for funding. We thank Prof. P. Ramamurthy and Dr. C. Selvaraju, NCUFP, University of Madras for lifetime measurements.

REFERENCES

1. V. Coropceanu, J. Cornil, D. A. da Silva Filho, Y. Olivier, R. Silbey and J.-L. Brédas, *Chemical Reviews*, 2007, 107, 926-952.
2. Y. Shirota and H. Kageyama, *Chemical Reviews*, 2007, 107, 953-1010.
3. J. Hwang, A. Wan and A. Kahn, *Materials Science and Engineering: R: Reports*, 2009, 64, 1-31.
4. M. G. Helander, Z. B. Wang, J. Qiu and Z. H. Lu, *Applied Physics Letters*, 2008, 93, 193310.
5. S. Zhong, J. Q. Zhong, H. Y. Mao, J. L. Zhang, J. D. Lin and W. Chen, *Physical Chemistry Chemical Physics*, 2012, 14, 14127-14141.
6. H.-L. Yip and A. K. Y. Jen, *Energy & Environmental Science*, 2012, 5, 5994-6011.
7. P. Škraba, G. Bratina, S. Igarashi, H. Nohira and K. Hirose, *Thin Solid Films*, 2011, 519, 4216-4219.
8. L. S. C. Pingree, B. A. MacLeod and D. S. Ginger, *The Journal of Physical Chemistry C*, 2008, 112, 7922-7927.
9. L. S. C. Pingree, B. A. MacLeod and D. S. Ginger, *The Journal of Physical Chemistry C*, 2008, 112, 7922-7927.
10. S. K. Hau, H.-L. Yip, J. Zou and A. K. Y. Jen, *Org Electron*, 2009, 10, 1401-1407.
11. J. Kettle, H. Waters, M. Horie and S. W. Chang, *Journal of Physics D: Applied Physics*, 2012, 45, 125102.
12. Z. a. Tan, D. Qian, W. Zhang, L. Li, Y. Ding, Q. Xu, F. Wang and Y. Li, *Journal of Materials Chemistry A*, 2013, 1, 657-664.
13. J. R. Manders, S.-W. Tsang, M. J. Hartel, T.-H. Lai, S. Chen, C. M. Amb, J. R. Reynolds and F. So, *Advanced Functional Materials*, 2013, 23, 2993-3001.
14. G. Li, C.-W. Chu, V. Shrotriya, J. Huang and Y. Yang, *Appl Phys Lett*, 2006, 88, 253503.
15. Y. Kanai, T. Matsushima and H. Murata, *Thin Solid Films*, 2009, 518, 537-540.
16. T. Yang, M. Wang, Y. Cao, F. Huang, L. Huang, J. Peng, X. Gong, S. Z. D. Cheng and Y. Cao, *Advanced Energy Materials*, 2012, 2, 523-527.
17. Z. a. Li, T. Ye, S. Tang, C. Wang, D. Ma and Z. Li, *Journal of Materials Chemistry C*, 2015, 3, 2016-2023.
18. N. Metri, X. Sallenave, C. Plesse, L. Beouch, P.-H. Aubert, F. Goubard, C. Chevrot and G. Sini, *The Journal of Physical Chemistry C*, 2012, 116, 3765-3772.
19. C.-Y. Chan, Y.-C. Wong, M.-Y. Chan, S.-H. Cheung, S.-K. So and V. W.-W. Yam, *Chemistry of Materials*, 2014, 26, 6585-6594.
20. J.-H. Huang and K.-C. Lee, *ACS Applied Materials & Interfaces*, 2014, 6, 7680-7685.
21. C.-Y. Hsu, Y.-C. Chen, R. Y.-Y. Lin, K.-C. Ho and J. T. Lin, *Physical Chemistry Chemical Physics*, 2012, 14, 14099-14109.
22. Z. Fang, V. Chellappan, R. D. Webster, L. Ke, T. Zhang, B. Liu and Y.-H. Lai, *Journal of Materials Chemistry*, 2012, 22, 15397-15404.
23. R. A. Klenkler and G. Voloshin, *The Journal of Physical Chemistry C*, 2011, 115, 16777-16781.
24. H. Choi, S. Paek, N. Lim, Y. H. Lee, M. K. Nazeeruddin and J. Ko, *Chemistry – A European Journal*, 2014, 20, 10894-10899.
25. P. Cias, C. Slugovc and G. Gescheidt, *The Journal of Physical Chemistry A*, 2011, 115, 14519-14525.
26. J. E. Kroeze, N. Hirata, L. Schmidt-Mende, C. Orizu, S. D. Ogier, K. Carr, M. Grätzel and J. R. Durrant, *Advanced Functional Materials*, 2006, 16, 1832-1838.
27. T. Leijtens, J. Lim, J. Teuscher, T. Park and H. J. Snaith, *Advanced Materials*, 2013, 25, 3227-3233.
28. G. Kron, T. Egerter, J. H. Werner and U. Rau, *The Journal of Physical Chemistry B*, 2003, 107, 3556-3564.
29. D. Poplavskyy and J. Nelson, *Journal of Applied Physics*, 2003, 93, 341-346.
30. P. Stakhira, S. Khomyak, V. Cherpak, D. Volyniuk, J. Simokaitiene, A. Tomkeviciene, N. A. Kukhta, J. V. Grazulevicius, A. V. Kukhta, X. W. Sun, H. V. Demir, Z. Hotra and L. Voznyak, *Synthetic Metals*, 2012, 162, 352-355.
31. E. Balasubramaniam, Y. T. Tao, A. Danel and P. Tomasik, *Chemistry of Materials*, 2000, 12, 2788-2793.
32. X.-C. Gao, H. Cao, L.-Q. Zhang, B.-W. Zhang, Y. Cao and C.-H. Huang, *Journal of Materials Chemistry*, 1999, 9, 1077-1080.
33. Z. Lu, Q. Jiang, W. Zhu, M. Xie, Y. Hou, X. Chen and Z. Wang, *Synthetic Metals*, 2000, 111–112, 465-468.
34. S. Takeshi, F. Takanori, N. Yoshitaka, H. Yuji, S. Kenichi and K. Kazuhiko, *Japanese Journal of Applied Physics*, 1995, 34, 3124.

35. X. H. Zhang, S. K. Wu, Z. Q. Gao, C. S. Lee, S. T. Lee and H. L. Kwong, *Thin Solid Films*, 2000, 371, 40-46.
36. P. M. Borsenberger and L. B. Schein, *The Journal of Physical Chemistry*, 1994, 98, 233-239.
37. R. B. Aher, G. Wanare, N. Kawathekar, R. R. Kumar, N. K. Kaushik, D. Sahal and V. S. Chauhan, *Bioorganic & Medicinal Chemistry Letters*, 2011, 21, 3034-3036.
38. S. Easwaramoorthi, B. Umamahesh, P. Cheranmadevi, R. S. Rathore and K. I. Sathiyanarayanan, *RSC Advances*, 2013, 3, 1243-1254.
39. W. H. Melhuish, *The Journal of Physical Chemistry*, 1961, 65, 229-235.
40. D. Vak, B. Lim, S.-H. Lee and D.-Y. Kim, *Organic Letters*, 2005, 7, 4229-4232.
41. A. M. Nardes, M. Kemerink, M. M. de Kok, E. Vinken, K. Maturova and R. A. J. Janssen, *Org Electron*, 2008, 9, 727-734.
42. H. Dong, H. Zhu, Q. Meng, X. Gong and W. Hu, *Chemical Society Reviews*, 2012, 41, 1754-1808.
43. J. Hirsch, *Journal of Physics C: Solid State Physics*, 1979, 12, 321.
44. B. C. Lin, C. P. Cheng, Z.-Q. You and C.-P. Hsu, *Journal of the American Chemical Society*, 2005, 127, 66-67.
45. X. Yang, L. Wang, C. Wang, W. Long and Z. Shuai, *Chemistry of Materials*, 2008, 20, 3205-3211.
46. N. S. Hush, *The Journal of Chemical Physics*, 1958, 28, 962-972.
47. R. A. Marcus, *Reviews of Modern Physics*, 1993, 65, 599-610.
48. J. Yin, S.-L. Zhang, R.-F. Chen, Q.-D. Ling and W. Huang, *Physical Chemistry Chemical Physics*, 2010, 12, 15448-15458.
49. A. G. Baboul, L. A. Curtiss, P. C. Redfern and K. Raghavachari, *The Journal of Chemical Physics*, 1999, 110, 7650-7657.
50. G. W. T. M. J. Frisch, H. B. Schlegel, G. E. Scuseria, M. A. Robb, J. R. Cheeseman, G. Scalmani, V. Barone, B. Mennucci, G. A. Petersson, H. Nakatsuji, M. Caricato, X. Li, H. P. Hratchian, A. F. Izmaylov, J. Bloino, G. Zheng, J. L. Sonnenberg, M. Hada, M. Ehara, K. Toyota, R. Fukuda, J. Hasegawa, M. Ishida, T. Nakajima, Y. Honda, O. Kitao, H. Nakai, T. Vreven, J. A. Montgomery, Jr., J. E. Peralta, F. Ogliaro, M. Bearpark, J. J. Heyd, E. Brothers, K. N. Kudin, V. N. Staroverov, R. Kobayashi, J. Normand, K. Raghavachari, A. Rendell, J. C. Burant, S. S. Iyengar, J. Tomasi, M. Cossi, N. Rega, J. M. Millam, M. Klene, J. E. Knox, J. B. Cross, V. Bakken, C. Adamo, J. Jaramillo, R. Gomperts, R. E. Stratmann, O. Yazyev, A. J. Austin, R. Cammi, C. Pomelli, J. W. Ochterski, R. L. Martin, K. Morokuma, V. G. Zakrzewski, G. A. Voth, P. Salvador, J. J. Dannenberg, S. Dapprich, A. D. Daniels, Ö. Farkas, J. B. Foresman, J. V. Ortiz, J. Cioslowski, and D. J. Fox, Gaussian, Inc., , *Gaussian, Inc.,Wallingford CT,*, 2009.
51. E. Varathan, D. Vijay and V. Subramanian, *The Journal of Physical Chemistry C*, 2014, 118, 21741-21754.
52. E. Varathan, D. Vijay, P. S. Vinod Kumar and V. Subramanian, *Journal of Materials Chemistry C*, 2013, 1, 4261-4274.
53. M.-K. Yan, Y. Tao, R.-F. Chen, C. Zheng, Z.-F. An and W. Huang, *RSC Advances*, 2012, 2, 7860-7867.
54. T. Koopmans, *Physica*, 1934, 1, 104-113.
55. G. P. Owen and A. Charlesby, *Journal of Physics C: Solid State Physics*, 1974, 7, L400.
56. V. K. C. Kao and W. Hwang, *Electrical transport in solids with particular reference to organic semiconductors*, Pergamon Press Oxford, 1981.
57. M. Planells, A. Abate, D. J. Hollman, S. D. Stranks, V. Bharti, J. Gaur, D. Mohanty, S. Chand, H. J. Snaith and N. Robertson, *Journal of Materials Chemistry A*, 2013, 1, 6949-6960.

Table of Contents Graphic